6002 *Biochemistry* **2009,** *48,* 6002–6011
DOI: 10.1021/bi900602h

BIOCHEMISTRY
including biophysical chemistry & molecular biology
Article

Pseudohyperphosphorylation Causing AD-like Changes in Tau Has Significant Effects on Its Polymerization[†]

Qian Sun and T. Chris Gamblin*

Department of Molecular Biosciences, University of Kansas, Lawrence, Kansas 66045

Received April 7, 2009; Revised Manuscript Received May 18, 2009

ABSTRACT: The microtubule-associated protein tau, in a hyperphosphorylated form, aggregates into insoluble paired-helical filaments (PHFs) in Alzheimer's disease (AD) and other tauopathies. In AD, there is approximately 8 mol of phosphate per mole of tau distributed among approximately 30 PHF phosphorylation sites as compared to 2−3 mol of phosphate per mole in normal brain. In AD, kinases such as glycogen synthase kinase-3β (GSK-3β) are believed to be involved in the generation of hyperphosphorylated tau. However, the functional consequences of hyperphosphorylation on the microtubule binding and polymerization of tau are not well understood. To address this question, we have generated pseudohyperphosphorylation mutants consisting of six and seven sites in the proline-rich region and carboxy terminus of tau by amino acid substitution. In addition, several single, double, and triple pseudophosphorylation mutants were also generated. Pseudophosphorylation of tau decreases its affinity for microtubules, and pseudohyperphosphorylated forms of tau do not have significantly decreased levels of microtubule binding as compared to single and double sites. Three pseudohyperphosphorylated forms of tau with altered sodium dodecyl sulfate−polyacrylamide gel electrophoresis migration have a greater effect on its inducer-mediated polymerization, slowing the rate of nucleation and elongation. On the basis of the observations that pseudohyperphosphorylated tau has decreased affinity for microtubules and reduced inducer-initiated rates of nucleation and polymerization, we propose that this combination could be the cause of the increased cytotoxicity of hyperphosphorylated tau in Alzheimer's disease and also explain the potentially beneficial role of tau polymerization and NFT formation.

Neurofibrillary tangles (NFTs)[1] are a prominent hallmark of Alzheimer's disease (AD) and other related neurodegenerative disorders, such as frontotemporal dementia and Parkinsonism linked to chromosome 17 (FTDP-17) (reviewed in ref (*1*)). Although the role of NFTs in Alzheimer's disease is not clear, the location and amount of NFTs directly correlate with the type and severity of cognitive impairment (*2*, *3*). NFTs contain large amounts of abnormal protein deposits in the form of straight and paired-helical filaments (*4*, *5*) that are composed almost entirely of the microtubule-associated protein tau (*6*−*9*) in a hyperphosphorylated state (*6*). Tau protein is a soluble protein that normally functions to promote the assembly and stabilization of the microtubule cytoskeleton (*10*), and phosphorylation of tau is known to alter its functions (reviewed in ref (*11*)). However, it is still unclear how tau hyperphosphorylation is linked to its aggregation and neuronal degeneration observed in these diseases.

At least 30 phosphorylation sites in PHF tau, approximately half of which are proline-directed sites, have been identified by mass spectrometry and phospho-amino acid analysis or by phosphorylation-specific monoclonal antibodies (reviewed in refs (*11*) and (*12*)). The kinase(s) responsible for the hyperphosphorylation of tau in AD is not clear. It has been suggested that more than one combination of kinases and/or phospatases might be involved in converting normal tau to hyperphosphorylated tau (*13*). The proline-directed kinase GSK-3β is believed to be involved in this process since it phosphorylates tau at many of the same sites that are found to be phosphorylated in paired-helical filaments of AD (*14*−*17*), and active GSK-3β is associated with the development of NFTs in AD (*18*). According to our previous observations, GSK-3β phosphorylates soluble and polymerized tau at a minimum of eleven and five sites, respectively (*19*, *20*). Phosphorylation at these sites does not change the amount of tau polymerization but is sufficient to cause tau filaments to coalesce into tanglelike aggregates similar to those isolated from Alzheimer's disease brain (*19*, *20*).

Because of the number and proximity of tau phosphorylation, in combination with the relative promiscuity with which most kinases act upon tau, the use of kinases to investigate the effects

[†]Support was provided by National Institutes of Health Grants AG022428 (T.C.G.) and AG025898 (T.C.G.).

*To whom correspondence should be addressed: Department of Molecular Biosciences, University of Kansas, 1200 Sunnyside Ave., Lawrence, KS 66045. Telephone: (785) 864-5065. Fax: (785) 864-5321. E-mail: gamblin@ku.edu.

[1]Abbreviations: AD, Alzheimer's disease; GSK-3β, glycogen synthase kinase-3β; TTK, tau-tubulin kinase; NFTs, neurofibrillary tangles; FTDP-17, frontotemporal dementia and Parkinsonism linked to chromosome 17; ARA, arachidonic acid; LLS, laser light scattering.

 Published on Web 05/21/2009

of specific sites on the function of tau is virtually impossible. It is therefore common for these investigations to employ site-directed mutagenesis to generate pseudophosphorylation variants of tau (*21*−*28*), although this approach is unlikely to completely mimic phosphorylative changes. We previously showed that the amino acid substitution of glutamic acid for serines or threonines to generate pseudophosphorylation mutations at S202 and T205 resulted in only subtle effects on the polymerization characteristics and microtubule binding of tau (*28*). However, it is not known whether adding additional pseudophosphorylation sites that are normally phosphorylated by GSK-3β to generate a "pseudohyperphosphorylation" version of tau has a greater effect on its function. To address this question, we have generated pseudohyperphosphorylated variants with six (6-phos) and seven (7-phos) pseudophosphorylation changes. The sites chosen for investigation include the five sites that are phosphorylated by GSK-3β when tau is in a polymerized state (S199, T205, T231, S396, and S404) (*20*). 6-phos also included pseudophosphorylation at S202. S202 was added to the five core sites since the AT8 antibody recognizes phosphorylation of tau at both S199 and S202 (*29*), and antibodies to S202 alone were not available for our previous study of GSK3β phosphorylation of tau. Similarly, S235, which is recognized in combination with T231 by the TG-3 antibody (*30*), was added to 6-phos to generate a 7-phos mutant. Single, double, and triple pseudophosphorylation mutants were also investigated to control for the possibility that fewer sites could have effects similar to those of the pseudohyperphosphorylated versions of tau. In addition to S199, S202, T205, T231, S235, S396, and S404, other sites were also investigated. T212E was included since it has previously be shown to promote the in vitro assembly of tau to a high level (*26*). S208D, S210D, and S208/210D were also included. These sites are not phosphorylated by GSK-3β but are in the same proline-rich region of tau in which the majority of GSK-3β phosphorylation sites are found. They are known to be phosphorylated by tau-tubulin kinase (TTK) (*31*) and are also phosphorylated in PHF tau (*32*). The pseudophosphorylation mutants were assayed for changes in SDS−PAGE migration, microtubule binding, and arachidonic acid-induced polymerization. We have made two key observations. Most pseudophosphorylation and pseudohyperphosphorylation variants decrease the level of microtubule binding of tau in a fashion similar to that of GSK-3β phosphorylated tau, and kinetic analyses of polymerization indicate that pseudohyperphosphorylated tau mimics with AD-like changes in sodium dodecyl sulfate−polyacrylamide gel electrophoresis (SDS−PAGE) electrophoretic mobility have increased lag times and reduced apparent rates of elongation compared to those of single or paired mimics. These results suggest a possible mechanism for the increased toxicity of hyperphosphorylated tau in vivo.

MATERIALS AND METHODS

Chemicals and Reagents. Arachidonic acid was obtained from Cayman Chemicals (Ann Arbor, MI), IPTG from Calbiochem (EMD Biosciences, La Jolla, CA), SDS−PAGE protein marker from Invitrogen (Gaithersburg, MD), and urea from Bio-Rad (Hercules, CA), and uranyl acetate and Formvar carbon-coated grids were obtained from Electron Microscopy Sciences (Hatfield, PA). Wild-type, P301L, and pseudophosphorylation mutant tau protein (441 amino acids) were expressed and purified as described previously (*28*). Pseudophosphorylation mutants were generated using the QuikChange site-directed mutagenesis kit from Stratagene (La Jolla, CA). S/T to E mutants and S/T to D mutants were generated at amino acids S199 and T231. S199E was found to have polymerization characteristics indistinguishable from thoso of S199D (not shown). T231E and T231D were also indistinguishable in their polymerization (not shown). The protein concentration was determined by a commercial BCA assay from Pierce Chemical (Rockford, IL) using bovine serum albumin (Pierce Chemical) as a standard.

SDS−PAGE and SDS−PAGE with Urea. Protein samples (1 μg per lane) were boiled for 5 min in sample buffer containing 2% SDS and 1% β-mercaptoethanol, fractionated via 15% SDS−PAGE, and stained with Coomassie brilliant blue (*33*). For denaturing SDS−PAGE, protein samples (1 μg per lane) were boiled for 5 min in sample buffer containing 2% SDS and 1% β-mercaptoethanol and 6 M urea. Samples were fractionated via 15% SDS−PAGE with 6 M urea and stained with Coomassie brilliant blue (*33*).

Kinetics of ARA-Induced Polymerization. Two micromolar tau protein (wild-type and pseudophosphorylation tau mutants) was incubated in polymerization buffer [10 mM HEPES (pH 7.64), 100 mM NaCl, 0.1 mM EDTA, and 5 mM DTT] at room temperature in the presence of 75 μM arachidonic acid (ARA) (in ethanol, final concentration of 3.75%) in the 5 mm × 5 mm optical glass fluorometer cuvettes (Starna Cells, Atascadero, CA) (*34*). The amount of polymerization was monitored by LLS at regular intervals for 20 h with a 5 mW solid state laser (λ = 475 nm) (B&W Tek, Inc., Newark, DE). Images were captured at a right angle to the incident light using a SONY XC-ST270 digital camera. Captured images were imported into Adobe Photoshop 7.0.1, and the intensity of the scattered light was measured as described previously (*28*). The pictures were captured at an aperture of f5.6−8 or f8 and then normalized to the intensity that corresponded to the exposure at f5.6−8. The data were fit to a nonlinear Gompertz function:

$$y = a\mathrm{e}^{-\mathrm{e}^{-\frac{t-t_i}{b}}}$$

where y is the value of laser light scattering measured at time t, a is the maximum amount of light scattering, t_i is the point of inflection where the increase in scattering is at its maximum, and b is equal to $1/k_{app}$. k_{app} is proportional to the rate of polymerization (*26*). The lag time for polymerization, or the amount of time required to observe significant amounts of polymerization, was calculated using the formula $t_i - b$ (*26*). The Gompertz function has been used as a model for growth curves (*35*), including as a model for tau polymerization (*26*). Errors in the kinetics parameters were assessed by individually fitting three separate kinetics experiments to the Gompertz function to yield three independent measures of LLS_{max}, k_{app}, and lag times. These values were averaged and reported with the standard deviation.

Transmission Electron Microscopy. Tau polymerization reaction mixtures were diluted 10-fold with polymerization buffer and then fixed with glutaraldehyde (final concentration of 2%) for 5 min. Ten microliters of fixed reactions was placed on Formvar carbon-coated grids (1 min), washed with water, blotted, washed with 2% uranyl acetate, blotted, stained with 2% uranyl acetate (1 min), and then blotted dry. Grids were viewed with a TECNAI G^2 20 electron microscope (FEI Co., Hillsboro, OR), and digital images were captured with the Gatan Digital Micrograph imaging system.

Microtubule Binding Assay. The microtubule binding assay was performed in general tubulin buffer [80 mM PIPES (pH 7),

1 mM $MgCl_2$, and 1 mM EGTA]. Tau protein at concentrations ranging from 0.125 to 10 μM was mixed with paclitaxel-stabilized microtubules at a final concentration of 1.62 μM tubulin dimer in a 50 μL reaction volume. Samples were incubated at room temperature for 30 min and centrifuged in a Beckman Optima TLX ultracentrifuge at 100000*g* for 5 min to sediment the microtubules and tau bound to the microtubules. The pellets were resuspended in SDS sample buffer, and microtubules were separated from tau bound to microtubules by SDS−PAGE. The concentration of tau bound to the microtubules was determined by the intensity of the tau band by Adobe Photoshop and normalized to the intensity of the tubulin band. The tau band was normalized to the intensity of the tubulin bands in each lane to account for any differences in centrifugation or resuspension of samples because the amount of tubulin should be constant in all binding reaction mixtures. The amount of free tau was determined by subtracting the amount of bound tau from the total amount of tau. The concentrations of bound tau were plotted versus the concentration of free tau in GraphPad Prism and fit to a one-site binding (hyperbola) equation.

RESULTS

Selection and Generation of Pseudophosphorylation Mutants. Hyperphosphorylated tau in Alzheimer's disease (AD) is phosphorylated at a molar ratio of approximately 5−9 mol of phosphate per mole of tau, whereas normal tau contains only 2−3 mol of phosphate per mole of tau (*36*). However, the role of this hyperphosphorylation is poorly understood. To improve our understanding of the effects of tau hyperphosphorylation, pseudophosphorylation mutants were constructed. We chose to focus on the five sites known to be phosphorylated by GSK-3β in vitro when arachidonic acid-induced tau filaments are used as the substrate (S199, T205, T231, S396, and S404) (*20*). Pseudophosphorylation changes at S202 were added to generate 6-phos, and both S202 and S235 were added to generate 7-phos (Figure 1A). These sites were included since S202 is often found phosphorylated along with S199 and S235 is often found phosphorylated along with T231. Single, paired, and triplet mutants were investigated to determine whether fewer sites might also have an effect on the function of tau (Figure 1A). We also investigated a GSK-3β site in the same proline-rich region but not among the sites above (T212) as a control. As further controls, non-proline-directed sites S208, S210, and S208/S210 were investigated. The disease-causing P301L tau mutation was included in the analyses as a positive control.

Pseudophosphorylation at S199/S202/T205, S396/S404, 6-phos, and 7-phos Induces AD-like Changes in Electrophoretic Mobility. Alzheimer's disease hyperphosphorylated tau and recombinant tau phosphorylated by GSK-3β in vitro have an upward band shift when analyzed by SDS−PAGE (*19*, *37*). This upward band shift is the definitive characteristic of hyperphosphorylated tau in neurodegenerative disorders (*1*). To determine whether the pseudophosphorylation mutants can cause this upward band shift, the pseudophosphorylation forms of tau were analyzed by coomassie-stained SDS−PAGE. S199/S202/T205E, S396/S404E, 6-phos, and 7-phos had an upward shift in mobility compared to wild-type tau (Figure 1B). The apparent molecular masses for the wild type, S199/S202/T205E, S396/S404E, 6-phos, and 7-phos were 70, 72, 75, 78, and 78 kDa, respectively. P301L tau and all other pseudophosphorylation mutants did not exhibit a change in mobility (data not shown). The mobility shift of pseudophosphorylation mutants was reduced in the presence of 6 M urea [molecular masses for the wild type, S199/S202/T205E, S396/S404E, 6-phos, and 7-phos of 70, 70, 71, 72, and 72 kDa, respectively (Figure 1C)]. This phenomenon of altered mobility in SDS that is abolished in urea has been described in the literature as a SDS-resistant change in conformation (*33*, *38*−*41*). Because S199/S202/T205E, S396/S404E, 6-phos, and 7-phos all demonstrated an AD-like shift in mobility as a result of phosphorylation-like changes, we conclude that they have the characteristics of hyperphosphorylated tau. These mutants will therefore be termed pseudohyperphosphorylated tau hereafter.

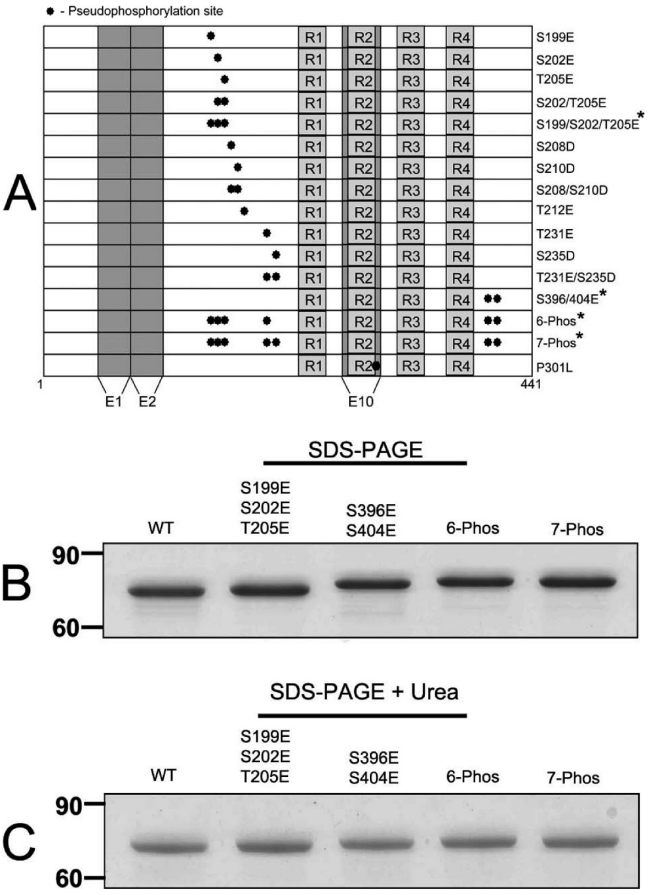

FIGURE 1: Simulation of phosphorylation by glutamate or aspartate replacement. (A) Diagram of phosphorylation sites on full-length tau. Four microtubule binding repeats are indicated by light gray boxes (R1−R4), and exons 2, 3, and 10 are indicated by dark gray boxes. Phosphorylation sites that have been mutated to glutamate or aspartate are indicated to the right of the diagram showing their position. The FTDP-17 mutant, P301L, is also indicated. The mutants with "hyperphosphorylation"-like changes are marked with an asterisk. (B) SDS-resistant upward band shifts were observed in the pseudophosphorylation mutants S199/S202/T202E, S396/S404E, 6-phos, and 7-phos. One microgram tau protein samples [wild-type tau (WT), S199/S202/T202E, S396/S404E, 6-phos, and 7-phos] were fractionated via SDS−PAGE on a 15% gradient gel. (C) SDS-resistant upward band shifts shown by S199/S202/T202E, S396/S404E, 6-phos, and 7-phos were reduced in the presence of 6 M urea. One microgram tau protein samples [wild-type tau (WT), S199/S202/T205E, S396/404E, 6-phos, and 7-phos] were fractionated via SDS−PAGE in a 15% gel made with 6 M urea.

Pseudophosphorylation of Tau Changes Its Affinity for Microtubules. Because FTDP-17 mutations (*42*) and pseudophosphorylation mutations (*28*) in tau can alter its interactions with microtubules, we measured the microtubule binding affinity

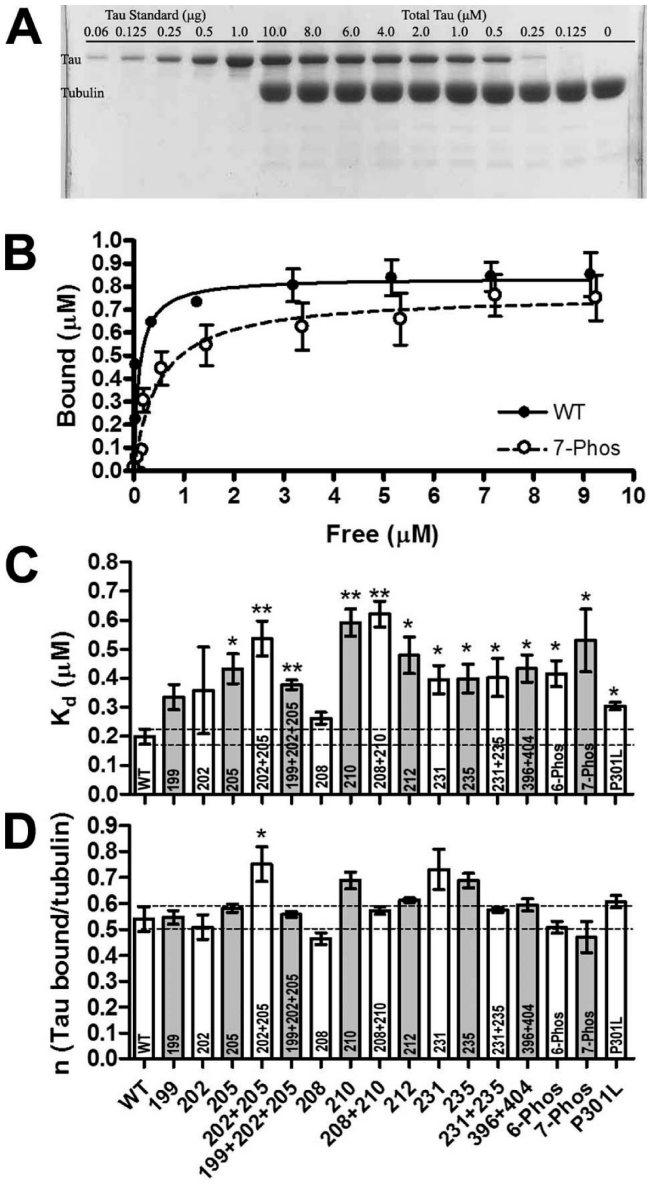

FIGURE 2: Microtubule binding of pseudophosphorylation mutants. The microtubule binding affinities of wild-type and mutant tau were measured using a centrifugal assay to separate bound and unbound tau. (A) Representative SDS−PAGE gel after centrifugation. The amounts of standard tau in the first five lanes are 0.06, 0.125, 0.25, 0.5, and 1 μg, respectively. Tau protein, at a concentration varying from 0 to 10 μM, was mixed with microtubules at a constant total MT concentration of 1.62 μM tubulin dimers. Bound tau was separated from free tau by centrifugation and fractionated via SDS−PAGE (lanes 6−15). (B) Two representative curves plotting the concentration of bound tau vs tau free in solution: (●) wild-type tau and (○) 7-phos tau. The amount of bound tau was determined by the intensity of the tau band via SDS−PAGE. The data were fit to a one-site binding equation. K_d and n were determined for each of three independent repetitions of the binding curves for each protein and are shown in panels C and D, respectively. All data are presented as the average of three independent determinations of K_d and n with the standard deviations ($n = 3$). Values that were significantly different from wild-type values at $p < 0.05$ (one asterisk) and $p < 0.01$ (two asterisks) were determined by a Student's t test.

of P301L tau and 15 pseudophosphorylation mutants using a centrifugation assay (*43*). Pellets containing microtubules and bound tau were resuspended in SDS sample buffer and analyzed by Coomassie-stained SDS−PAGE (Figure 2A). The concentration of tau bound to the microtubules was determined by the intensity of the tau band and normalized to the intensity of the tubulin band (Figure 2A). Normalization of the amount of tau relative to tubulin was performed to take into account any differences in sedimentation or resuspension of the pellets. The concentration of free tau was calculated by subtracting the measured amount of bound tau from the total amount of tau added to the reaction mixture. The amount of bound tau was plotted against the amount of free tau. Two representative curves (wild-type tau and 7-phos) are shown in Figure 2B. The data were fit to a simple one-site binding equation to determine the affinity of binding (K_d) and the maximal amount of bound tau (B_{max}) (Figure 2C,D). All proteins examined, with the exception of S199E, S202E, and S208D, had affinities for microtubules significantly lower than that observed with wild-type tau (Figure 2B). The decreases in binding affinity were all in the 2−3-fold reduction range, which is in general agreement with previously published reports of GSK-3β phosphorylation of tau (*44*) and the P301L mutation (*42*). The stoichiometry of binding to microtubules was not greatly affected (Figure 2C).

Pseudophosphorylation Influences the Arachidonic Acid Induction of Tau Polymerization. To determine whether pseudophosphorylation mutations of tau have an effect on the arachidonic acid (ARA) induction of tau polymerization, each protein at a final concentration of 2 μM was incubated in the presence of 75 μM ARA. This protein:inducer ratio was chosen since it has been shown to be the optimal condition for the arachidonic acid induction of wild-type tau polymerization (*34*). The kinetics of polymerization of each mutant were followed by right angle laser light scattering and compared to those of wild-type tau. Representative curves are shown in Figure 3A. The data were fit to a Gompertz function to determine the maximal amount of light scattering (LLS_{max}) (Figure 3B), the apparent proportional growth rate [k_{app} (Figure 3C)], and the lag time of polymerization (Figure 3D). No significant increases in the degree of polymerization were observed for the pseudophosphorylation mutants (Figure 3B), although the FTDP-17 mutation P301L did have a significant increase in the extent of polymerization compared to that of the wild type, as expected (*45*). Several pseudophosphorylation variants (S202/T205E, S199/S202/T205E, S208/S210D, T231E, S396/S404E, 6-phos, and 7-phos) had significantly less maximal polymerization than the wild type.

The apparent proportional growth rate, k_{app}, was not significantly altered for most of the mutants (Figure 3C). The FTDP-17 mutation P301L has been shown to have the most dramatic effects in increasing the apparent rate of polymerization as compared to wild-type tau protein (*45*) and had a k_{app} significantly greater than that of wild-type tau and all the pseudophosphorylation mutants. Mutants S210D and T231D also had k_{app} values significantly greater than that of the wild type, but still less than that of P301L tau (Figure 3C). S199/S202/T205E, 6-phos, and 7-phos all had k_{app} values significantly lower than that of wild-type tau (Figure 3C).

Nucleation−elongation polymerization pathways are also typically characterized by a lag time in the polymerization process. Wild-type tau had a lag time of 19 min (Figure 3D). P301L tau had a significantly reduced lag time, as expected (*45*). S210D, S208/S210D, T231E, and T231E/S235D also had significantly reduced lag times, but greater than that of P301L tau (Figure 3D). 6-phos had a significantly longer lag time than wild-type tau (Figure 3D). On average, S199/S202/T205E and 7-phos

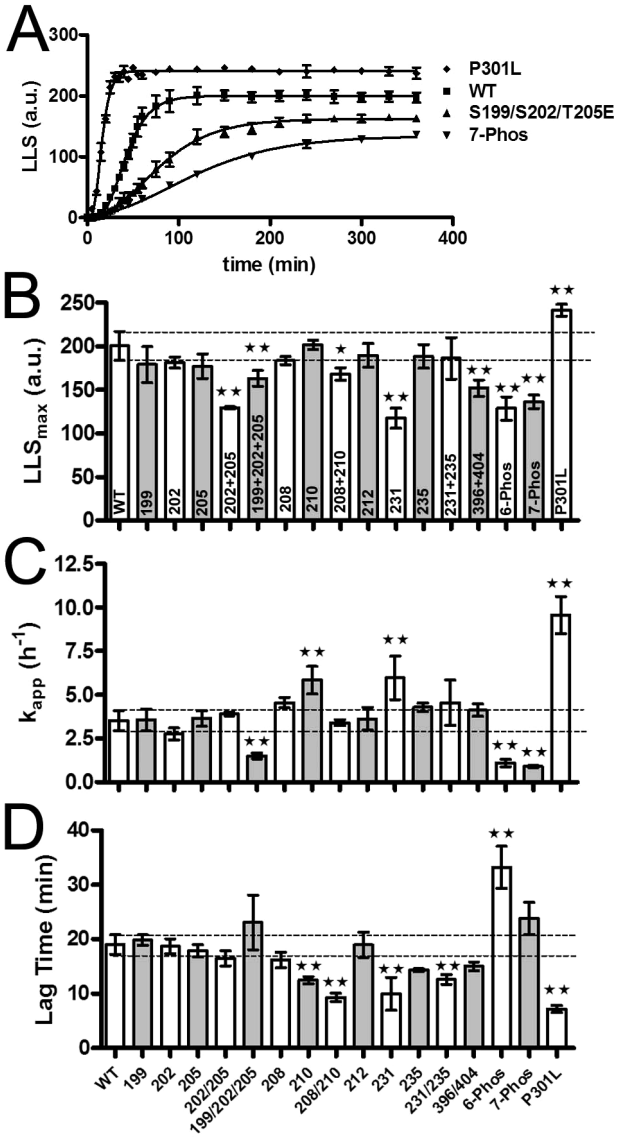

FIGURE 3: Kinetics of ARA induction of tau polymerization. The kinetics of wild-type and mutant tau polymerization at 2 μM protein and 75 μM ARA inducer were monitored by laser light scattering. (A) Four representative averaged curves of the amount of light scattering (LLS) at the times indicated are shown for (■) the wild type, (▲) S199/S202/T205E, (▼) 7-phos, and (◆) P301L. Each experimental data set was fit to a Gompertz function. LLS_{max}, k_{app}, and lag time were determined from the equation as described in Materials and Methods and are shown in panels B−D, respectively. All data are presented as averaged values ± the standard deviation from the three independent data sets. Values that were significantly different from wild-type values at $p < 0.05$ (one asterisk) and $p < 0.01$ (two asterisks) were determined by one-way ANOVA analysis of variance with Dunnett's multiple comparison post test using the wild type as the control column.

had longer lag times than the wild type, but these differences did not reach statistical significance (Figure 3D).

Pseudophosphorylation Changes the Morphology of ARA-Induced Tau Filaments. To determine whether filament morphology (number and length of filaments) was changed by pseudophosphorylation, samples from polymerization reactions were prepared and viewed by TEM (Figure 4). Filaments from six fields of view were combined into a single data set and then ranked according to their length (examples shown in Figure 5A). Particles less than 15 nm in their longest dimension were not included in the analysis because particles smaller than this cutoff value are smaller than the average filament width of arachidonic acid-induced filaments (*19*) and therefore difficult to distinguish from background. In general, pseudophosphorylation mutants tended to form fewer but longer filaments than wild-type tau (Figure 5B,C). The standard deviation of the average lengths was roughly equal to the value of the average lengths for most proteins, as is expected for exponentially distributed data (*46*). The standard error of the mean is also shown, as this is an estimate of the accuracy of the determination of the true mean. Among these mutants, the three with the most phosphorylation sites formed the longest filaments (S199/S202/T20E5, 6-phos, and 7-phos) (Figure 5C). However, the overall amount of filament formation observed in six fields was relatively similar for almost all proteins (Figure 5D), with the possible exceptions of T231E, S202/T205E, T205E, and S396/404E which seemed to have somewhat reduced levels of polymerization compared to the other proteins (Figure 5D). In general, pseudophosphorylation of tau resulted in fewer but longer filaments as compared to those of the wild type (Figures 4 and 5). In contrast, the rapidly polymerizing P301L formed more but shorter filaments than wild-type tau, resulting in an overall increase in the amount of polymerized material (Figure 5A−D).

Quantitative analysis of differences between the filaments is difficult due to the differences in the number of filaments, the variability in filament distribution on the TEM grid, the biological variability in filament lengths, and the exponential distribution of filament lengths. Therefore, it is possible that the apparent differences in filament length distributions (Figure 5) could be due to differences in sampling. We therefore measured 500 filaments for each mutant and determined the number-average length [$L_n = (\sum N_i L_i)/(\sum N_i)$ (Figure 6)] for each mutant (*47*). With the exception of T231E, all pseudophosphorylation mutants had greater average filament lengths than the wild-type protein. This analysis also confirmed that S199/S202/T205E, 6-phos, and 7-phos had the strongest tendencies to form long filaments.

DISCUSSION

Significance of Pseudophosphorylation Mutant Sites. Hyperphosphorylation of the microtubule-associated protein tau is a pathological hallmark of Alzheimer's disease and other tauopathies. Many kinases have been shown to be involved in this phosphorylation process, and GSK-3β is believed to be a major contributor to tau/PHF phosphorylation (reviewed in ref (*11*)). In previous studies, we found that GSK-3β phosphorylation of preformed tau filaments at sites, including S199, T205, T231, S396, and S404, can cause tau filaments to coalesce into NFT-like structures (*20*). Because these five sites are recognized by specific AD-associated antibodies, we sought to test whether pseudophosphorylation at these sites would have an impact on the function of tau (summarized in Table 1).

Role of Phosphorylation in Tau Polymerization. Phosphorylation of tau at specific sites has been suggested to correlate with the formation of neurofibrillary tangles (NFTs), raising the possibility that a major function of tau phosphorylation is to promote tau polymerization (*48*). Under conditions that we have determined to be optimal for wild-type tau polymerization (*34*), pseudophosphorylation of tau mildly reduced its degree of polymerization, which is consistent with previously published reports using in vitro GSK-3β phosphorylated tau (*19*, *49*). The kinetics of polymerization for most of the single and double phosphorylation variants were

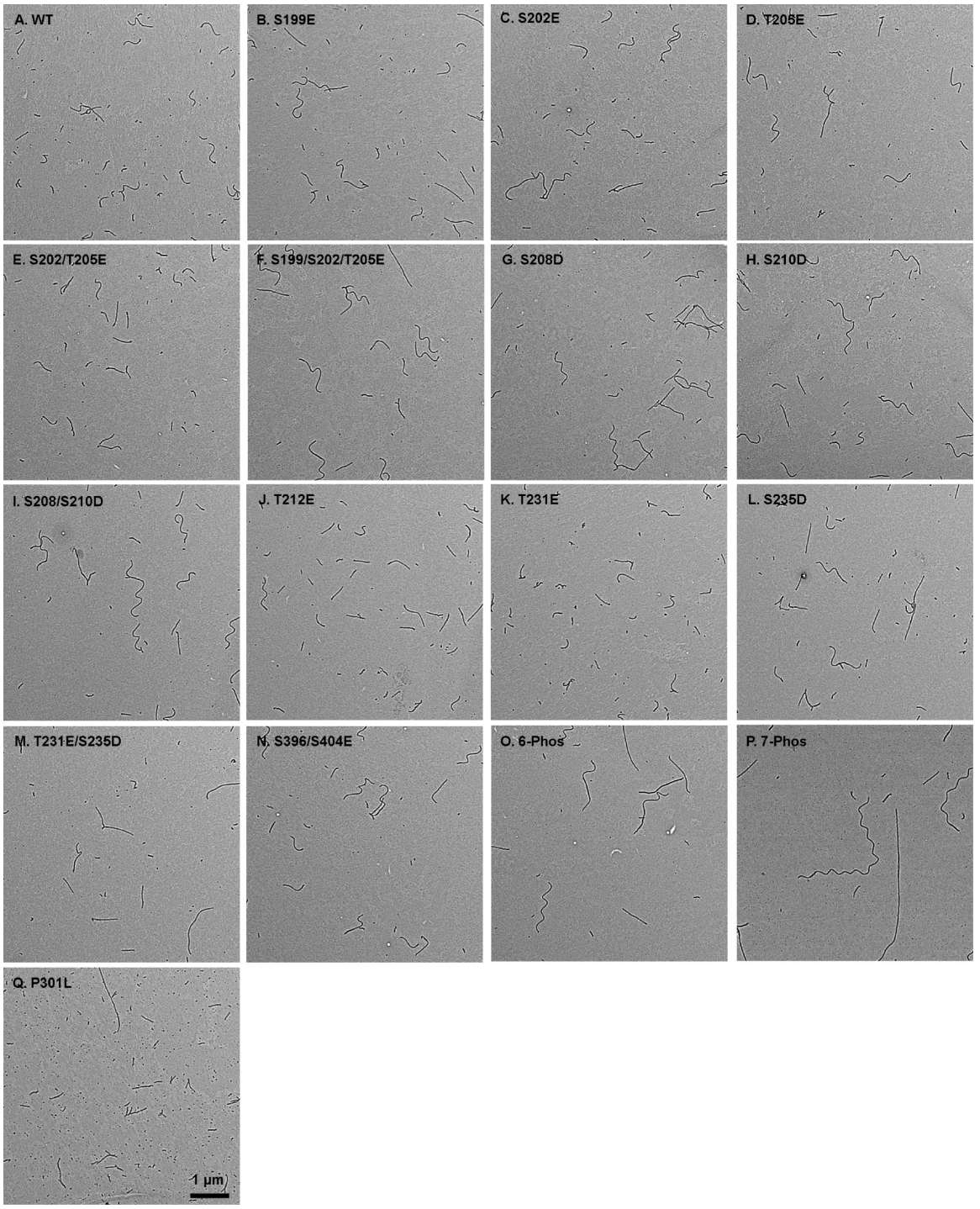

FIGURE 4: TEM analysis of polymerization at final concentrations of 2 μM tau protein and 75 μM ARA inducer. The polymerizations of wild-type and mutant tau at 2 μM protein and 75 μM ARA inducer were viewed by TEM after incubation for 20 h at room temperature. Representative micrographs are shown: (A) wild type, (B) S199E, (C) S202E, (D) T205E, (E) S202/T205E, (F) S199/S202/T205E, (G) S208D, (H) S210D, (I) S208/S210D, (J) T212E, (K) T231E, (L) S235D, (M) T231E/S235D, (N) S396/S404E, (O) 6-phos, (P) 7-phos, and (Q) P301L. The scale bar in panel Q represents 500 nm and is applicable to all images.

not significantly changed (Table 1). However, the pseudohyperphosphorylated version of tau (S199/S202/T205E, 6-phos, and 7-phos) had a drastically decreased rate of elongation and a pronounced lag time. This suggests a deficiency in the nucleation step for the pseudohyperphosphorylation mimics. The observation of fewer but longer filaments with pseudohyperphosphorylation mutants agrees with this idea.

The effect on filament nucleation and filament length was greatest with the pseudohyperphosphorylated versions of tau. 6-phos and 7-phos were generated from the combination of multiple pseudophosphorylation sites in both the proline-rich and C-terminal regions of tau. The effects on polymerization of 6-phos and 7-phos seem to be greater than those observed by the heparin (*49*) or arachidonic acid (*19*) induction of GSK-3β-phosphorylated tau polymerization. However, GSK-3β phosphorylation in vitro only results in 2−4 mol of phosphate incorporation per mole of tau distributed unequally over as many as 14 sites (*19*, *20*, *49*−*51*). 6-phos and 7-phos are homogeneous in

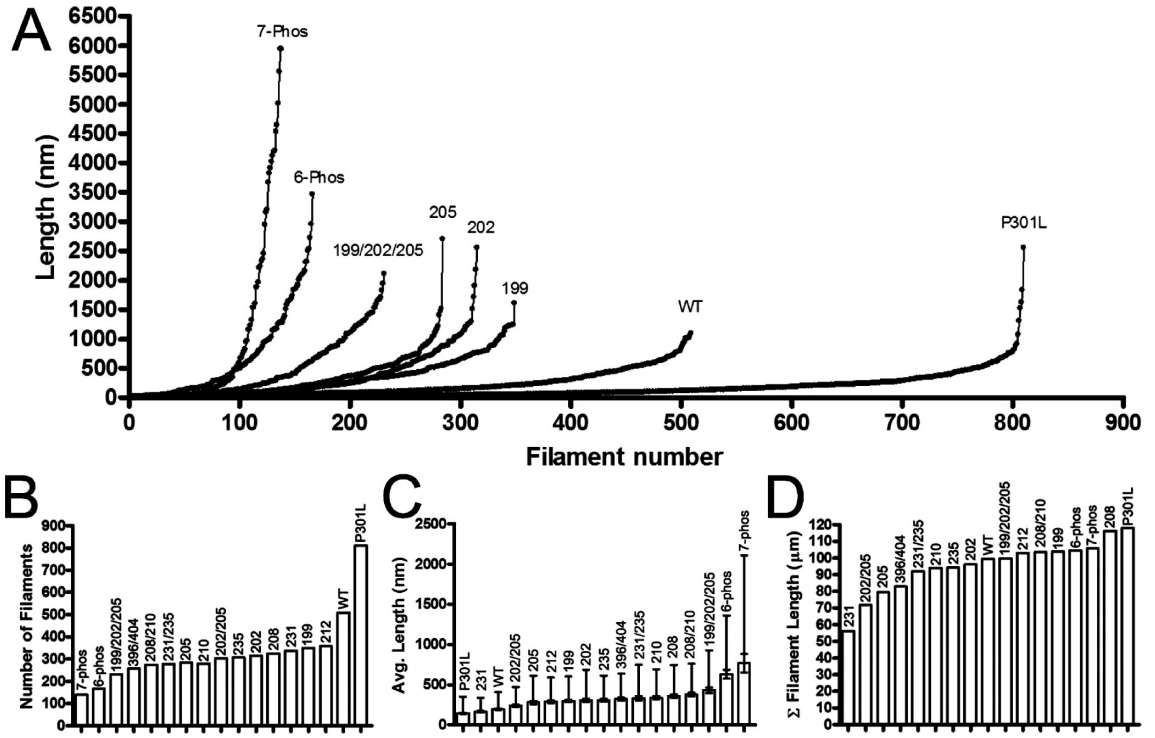

FIGURE 5: Filament distribution of polymerization at final concentrations of 2 μM tau protein and 75 μM ARA inducer. The polymerizations of wild-type and mutant tau at 2 μM protein and 75 μM ARA inducer were viewed by TEM after incubation for 20 h at room temperature. Resulting filament lengths were measured using Optimas image analysis software. Six 36 μm^2 fields were analyzed for each protein. (A) The filament lengths were combined into a single data set and ranked from shortest to longest. Each individual filament length was plotted against its corresponding rank for each protein. Several examples are shown and are individually labeled on the graph. The distributions for S210D, S208/S210D, T231E/S235D, and S396/S404E were similar to that of T205E. The distributions for S202/T205E, S208D, and S235D were similar to that of S202E. The distributions for T212E and T231E were similar to that of S199E. (B) Total number of filaments observed in six 36 μm^2 fields in ranked order from least to greatest. Each bar is individually labeled on the graph. (C) Average length of the filaments observed in six 36 μm^2 fields in ranked order from least to greatest. Each bar is individually labeled on the graph. Values are shown as averages ± the standard deviation (error bars above only) and ± the standard error of the mean (bars above and below). (D) Sum of all filament lengths from six 36 μm^2 fields in ranked order from least to greatest. Each bar is individually labeled on the graph.

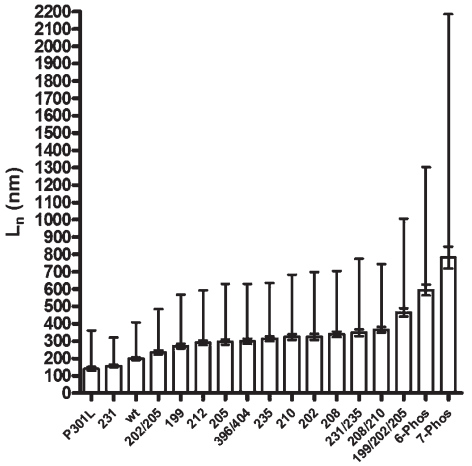

FIGURE 6: Pseudophosphorylation mutants form longer filaments than wild-type tau. Wild-type and mutant tau protein (2 μM) were incubated in polymerization buffer with 75 μM ARA for 20 h. Resulting filament lengths for 500 filaments were measured using Optimas image analysis software. The number-average lengths ± the standard deviation (error bars above) and ± the standard error of the mean (error bars above and below) for each protein were ranked by their average length and are labeled on the *x*-axis.

their modifications and therefore are more highly modified than the average GSK-3β-phosphorylated tau protein.

Our previous studies have shown that the presence of arachidonic acid drastically reduces the energetic barrier for the nucleation of polymerization (*34*). The observation that pseudohyperphosphorylation mutants are less likely to nucleate could be explained by weakened interactions with arachidonic acid as a result of altered conformations of the proteins conferred by pseudophosphorylation. In support of this, the pseudohyperphosphorylated proteins had altered SDS−PAGE electrophoretic mobility that was abolished in the presence of urea. This phenomenon has been described as an SDS-resistant change in the conformation of tau (*33*, *38*−*41*) and indicates that pseudophosphorylated proteins could interact differently with SDS or with arachidonic acid.

It should be mentioned that a previous report found that pseudophosphorylation of tau at several sites (including S199, S199/S202/T205, and T212) enhanced polymerization by 2−3-fold over nonmodified tau (*26*). We obtain similar results when using concentrations of arachidonic acid that inhibit wild-type tau polymerization [125−150 μM (data not shown)]. It is not clear whether these results at high inducer:protein ratios have physiological relevance, but they are consistent with the hypothesis that pseudophosphorylation of tau can weaken its interactions with arachidonic acid.

Role of Phosphorylation in Microtubule Binding. Most pseudophosphorylation forms of tau significantly decreased the level of microtubule binding by 2−3-fold without significantly changing the saturation levels (Table 1), which agrees with previous studies investigating the effects of tau phosphorylation at proline-directed phosphorylation sites (*49*).

Table 1: Summary of Effects of Pseudophosphorylation on Tau Function Compared to the Wild Type[a]

		microtubule binding		kinetics of polymerization			EM[g]	
protein	SDS band shift	K_d[b]	n[c]	LLS_{max}[d]	k_{app}[e]	lag time[f]	average L[h]	C_σ[i]
WT	no	0.20 ± 0.04	0.54 ± 0.08	200 ± 16	3.5 ± 0.6	19.0 ± 1.8	198	1.06
S199E							271	1.09
S202E							325	1.15
S208D							339	1.08
T212E		▲					291	1.04
T205E		▲					295	1.14
S235D		▲					314	1.02
231,235		▲				▼▼	348	1.23
S210D		▲▲			▲▲	▼▼	323	1.11
208,210		▲▲		▼		▼▼	365	1.04
396,404	▲	▲		▼▼			300	1.10
202,205		▲▲	▲	▼▼			235	1.07
T231E		▲		▼▼	▲▲	▼▼	156	1.05
199,202,205	▲	▲▲		▼▼	▼▼		466	1.16
7-phos	▲	▲		▼▼	▼▼		781	1.80
6-phos	▲	▲		▼▼	▼▼	▲▲	594	1.19
P301L		▲		▲▲	▲▲	▼▼	141	1.58

[a] Pseudophosphorylation variants are ranked by number of significant changes as compared to the wild type. Triangles represent increases (▲) or decreases (▼) in values as compared to that of wild type. A single triangle represents $p > 0.05$, and two triangles represent $p > 0.01$. The number of triangles does not represent the magnitude of the change. [b] K_d, dissociation constant (μM ± standard deviation). [c] n, maximal level of tau binding per tubulin molecule ([tau]/[tubulin]). [d] LLS_{max}, maximum amount of right angle laser light scattering after polymerization for ~20 h in arbitrary units ± standard deviation. [e] k_{app}, proportional growth rate of filaments in units of h^{-1} ± standard deviation. [f] Lag time, approximate time (in minutes) before significant polymerization was detected ± standard deviation. [g] EM, electron microscopy. [h] Average L, number-average length of filaments in nanometers determined by measuring the lengths of 500 filaments ± standard deviation. [i] C_σ, coefficient of variation that is equal to the mean divided by the standard deviation. For exponential length distributions, the average length is expected to be approximately equal to the standard deviation (*46*), or a C_σ of ~1.0.

However, results from multiple site constructs were not consistently additive. For example, both T231E and S235D had lower affinities than the wild type for microtubules. However, the T231E/S235D double mutant had an affinity similar to those of the individual mutations, and while S202/T205E had a lower affinity for microtubules than the individual mutants, the addition of S199E to form S199/S202/T205E actually improved microtubule binding (albeit at an affinity lower than that of wild-type tau). The constructs with six or seven pseudophosphorylation sites did not exhibit dramatically different levels of microtubule binding versus single or double mutants. We conclude that microtubule binding is regulated in a complicated site-specific fashion, and the levels of phosphorylation play a lesser role as a determinant of microtubule binding than the actual sites involved.

Phosphorylation, Polymerization, NFTs, and Toxicity. Since the establishment of the correlation between the number of NFTs with the degree of dementia in AD, NFTs have been widely accepted as a toxic species in AD (reviewed in ref (*52*)). However, recent observations in tau-expressing cultured cell, transgenic *Drosophila*, and mouse models suggest that the toxicity is independent of NFT formation and NFTs may form as a result of cellular attempts to reduce toxicity (reviewed in ref (*53*)). NFTs contain large amounts of abnormal hyperphosphorylated tau (*6*) in the form of straight and paired-helical filaments (*4*, *5*). The abnormal hyperphosphorylation of tau is one of the post-translational modifications of tau known to be related to toxicity, filament formation, and the formation of NFTs (reviewed in ref (*54*)). The apparent phosphorylation-dependent toxicity of tau could be due to the disruption of microtubule dynamics through sequestration of normal tau (*55*−*57*) and could be reduced through the polymerization of phosphorylated tau (*58*). Additionally, the presence of soluble hyperphosphorylated tau is correlated with cognitive deficiencies in a transgenic mouse model (*59*). These results suggest that tau aggregation could protect against phosphorylation-induced microtubule disruption and subsequent neurodegeneration.

Our results provide a potential biochemical mechanism for the potential cytotoxicity of hyperphosphorylated tau. Phosphorylated tau binds to microtubules less tightly, so that there would be an increase in the level of cytoplasmic tau and increased microtubule instability. It has also been shown through other work that hyperphosphorylated tau may sequester normal tau (*56*), further disrupting microtubule dynamics. Pseudohyperphosphorylated tau also has a decreased rate of polymerization, potentially increasing the amount of time it is soluble in the cytoplasm where it could sequester normal tau. It is also possible that the fibrillization of abnormally phosphorylated tau could protect cells from toxic effects. We have previously shown tau phosphorylation by GSK-3β is sufficient to induce the bundling of tau filaments into NFT-like structures in a cell-free in vitro system (*20*). These observations are consistent with data from transgenic mouse models showing that NFT formation is not necessarily the toxic element of neurodegeneration and may instead play a protective role (*59*−*61*).

ACKNOWLEDGMENT

We thank Carolyn Rankin and Kellen Voss for critical reading of the manuscript. We also thank Mike Branden for protein production.

REFERENCES

(1) Sergeant, N., Delacourte, A., and Buee, L. (2005) Tau protein as a differential biomarker of tauopathies. *Biochim. Biophys. Acta 1739*, 179–197.
(2) Arriagada, P. V., Growdon, J. H., Hedley-Whyte, E. T., and Hyman, B. T. (1992) Neurofibrillary tangles but not senile plaques parallel duration and severity of Alzheimer's disease. *Neurology 42*, 631–639.
(3) McKee, A. C., Kosik, K. S., and Kowall, N. W. (1991) Neuritic pathology and dementia in Alzheimer's disease. *Ann. Neurol. 30*, 156–165.

(4) Kidd, M. (1963) Paired helical filaments in electron microscopy of Alzheimer's disease. *Nature 197*, 192–193
(5) Yagishita, S., Itoh, Y., Nan, W., and Amano, N. (1981) Reappraisal of the fine structure of Alzheimer's neurofibrillary tangles. *Acta Neuropathol. 54*, 239–246
(6) Grundke-Iqbal, I., Iqbal, K., Tung, Y. C., Quinlan, M., Wisniewski, H. M., and Binder, L. I. (1986) Abnormal phosphorylation of the microtubule-associated protein tau (tau) in Alzheimer cytoskeletal pathology. *Proc. Natl. Acad. Sci. U.S.A. 83*, 4913–4917
(7) Kondo, J., Honda, T., Mori, H., Hamada, Y., Miura, R., Ogawara, M., and Ihara, Y. (1988) The carboxyl third of tau is tightly bound to paired helical filaments. *Neuron 1*, 827–834
(8) Kosik, K. S., Joachim, C. L., and Selkoe, D. J. (1986) Microtubule-associated protein tau (tau) is a major antigenic component of paired helical filaments in Alzheimer's disease. *Proc. Natl. Acad. Sci. U.S.A. 83*, 4044–4048
(9) Wischik, C. M., Novak, M., Thogersen, H. C., Edwards, P. C., Runswick, M. J., Jakes, R., Walker, J. E., Milstein, C., Roth, M., and Klug, A. (1988) Isolation of a fragment of tau derived from the core of the paired helical filament of Alzheimer disease. *Proc. Natl. Acad. Sci. U.S.A. 85*, 4506–4510
(10) Weingarten, M. D., Lockwood, A. H., Hwo, S. Y., and Kirschner, M. W. (1975) A protein factor essential for microtubule assembly. *Proc. Natl. Acad. Sci. U.S.A. 72*, 1858–1862
(11) Stoothoff, W. H., and Johnson, G. V. (2005) Tau phosphorylation: Physiological and pathological consequences. *Biochim. Biophys. Acta 1739*, 280–297.
(12) Buee, L., Bussiere, T., Buee-Scherrer, V., Delacourte, A., and Hof, P. R. (2000) Tau protein isoforms, phosphorylation and the role in neurodegenerative disorders. *Brain Res. Brain Res. Rev. 33*, 95–130.
(13) Wang, J. Z., Grundke-Iqbal, I., and Iqbal, K. (2007) Kinases and phosphatases and tau sites involved in Alzheimer neurofibrillary degeneration. *Eur. J. Neurosci. 25*, 59–68.
(14) Balaraman, Y., Limaye, A. R., Levey, A. I., and Srinivasan, S. (2006) Glycogen synthase kinase 3β and Alzheimer's disease: Pathophysiological and therapeutic significance. *Cell. Mol. Life Sci. 63*, 1226–1235.
(15) Illenberger, S., Zheng-Fischhofer, Q., Preuss, U., Stamer, K., Baumann, K., Trinczek, B., Biernat, J., Godemann, R., Mandelkow, E. M., and Mandelkow, E. (1998) The endogenous and cell cycle-dependent phosphorylation of tau protein in living cells: Implications for Alzheimer's disease. *Mol. Biol. Cell 9*, 1495–1512.
(16) Song, J. S., and Yang, S. D. (1995) Tau protein kinase I/GSK-3β/kinase FA in heparin phosphorylates tau on Ser199, Thr231, Ser235, Ser262, Ser369, and Ser400 sites phosphorylated in Alzheimer disease brain. *J. Protein Chem. 14*, 95–105.
(17) Wang, J. Z., Wu, Q., Smith, A., Grundke-Iqbal, I., and Iqbal, K. (1998) Tau is phosphorylated by GSK-3 at several sites found in Alzheimer disease and its biological activity markedly inhibited only after it is prephosphorylated by A-kinase. *FEBS Lett. 436*, 28–34.
(18) Leroy, K., Yilmaz, Z., and Brion, J. P. (2007) Increased level of active GSK-3β in Alzheimer's disease and accumulation in argyrophilic grains and in neurones at different stages of neurofibrillary degeneration. *Neuropathol. Appl. Neurobiol. 33*, 43–55.
(19) Rankin, C. A., Sun, Q., and Gamblin, T. C. (2007) Tau phosphorylation by GSK-3β promotes tangle-like filament morphology. *Mol. Neurodegener. 2*, 12.
(20) Rankin, C. A., Sun, Q., and Gamblin, T. C. (2008) Pre-assembled tau filaments phosphorylated by GSK-3b form large tangle-like structures. *Neurobiol. Dis. 31*, 368–377.
(21) Abraha, A., Ghoshal, N., Gamblin, T. C., Cryns, V., Berry, R. W., Kuret, J., and Binder, L. I. (2000) C-Terminal inhibition of tau assembly in vitro and in Alzheimer's disease. *J. Cell Sci. 113* (Part 21), 3737–3745
(22) Ding, H., Matthews, T. A., and Johnson, G. V. (2006) Site-specific phosphorylation and caspase cleavage differentially impact tau-microtubule interactions and tau aggregation. *J. Biol. Chem. 281*, 19107–19114
(23) Fath, T., Eidenmuller, J., and Brandt, R. (2002) Tau-mediated cytotoxicity in a pseudohyperphosphorylation model of Alzheimer's disease. *J. Neurosci. 22*, 9733–9741
(24) Haase, C., Stieler, J. T., Arendt, T., and Holzer, M. (2004) Pseudophosphorylation of tau protein alters its ability for self-aggregation. *J. Neurochem. 88*, 1509–1520
(25) Necula, M., Chirita, C. N., and Kuret, J. (2005) Cyanine dye N744 inhibits tau fibrillization by blocking filament extension: Implications for the treatment of tauopathic neurodegenerative diseases. *Biochemistry 44*, 10227–10237.
(26) Necula, M., and Kuret, J. (2004) Pseudophosphorylation and glycation of tau protein enhance but do not trigger fibrillization in vitro. *J. Biol. Chem. 279*, 49694–49703.
(27) Necula, M., and Kuret, J. (2005) Site-specific pseudophosphorylation modulates the rate of tau filament dissociation. *FEBS Lett. 579*, 1453–1457.
(28) Rankin, C. A., Sun, Q., and Gamblin, T. C. (2005) Pseudo-phosphorylation of tau at Ser202 and Thr205 affects tau filament formation. *Brain. Res. Mol. Brain Res. 138*, 84–93.
(29) Biernat, J., Mandelkow, E. M., Schroter, C., Lichtenberg-Kraag, B., Steiner, B., Berling, B., Meyer, H., Mercken, M., Vandermeeren, A., and Goedert, M.; et al. (1992) The switch of tau protein to an Alzheimer-like state includes the phosphorylation of two serine-proline motifs upstream of the microtubule binding region. *EMBO J. 11*, 1593–1597
(30) Jicha, G. A., Lane, E., Vincent, I., Otvos, L.Jr., Hoffmann, R., and Davies, P. (1997) A conformation- and phosphorylation-dependent antibody recognizing the paired helical filaments of Alzheimer's disease. *J. Neurochem. 69*, 2087–2095
(31) Tomizawa, K., Omori, A., Ohtake, A., Sato, K., and Takahashi, M. (2001) Tau-tubulin kinase phosphorylates tau at Ser-208 and Ser-210, sites found in paired helical filament-tau. *FEBS Lett. 492*, 221–227
(32) Hanger, D. P., Betts, J. C., Loviny, T. L., Blackstock, W. P., and Anderton, B. H. (1998) New phosphorylation sites identified in hyperphosphorylated tau (paired helical filament-tau) from Alzheimer's disease brain using nanoelectrospray mass spectrometry. *J. Neurochem. 71*, 2465–2476
(33) Eidenmuller, J., Fath, T., Maas, T., Pool, M., Sontag, E., and Brandt, R. (2001) Phosphorylation-mimicking glutamate clusters in the proline-rich region are sufficient to simulate the functional deficiencies of hyperphosphorylated tau protein. *Biochem. J. 357*, 759–767.
(34) Carlson, S. W., Branden, M., Voss, K., Sun, Q., Rankin, C. A., and Gamblin, T. C. (2007) A complex mechanism for inducer mediated tau polymerization. *Biochemistry 46*, 8838–8849.
(35) Winsor, C. P. (1932) The Gompertz Curve as a Growth Curve. *Proc. Natl. Acad. Sci. U.S.A. 18*, 1–8.
(36) Kopke, E., Tung, Y. C., Shaikh, S., Alonso, A. C., Iqbal, K., and Grundke-Iqbal, I. (1993) Microtubule-associated protein tau. Abnormal phosphorylation of a non-paired helical filament pool in Alzheimer disease. *J. Biol. Chem. 268*, 24374–24384.
(37) Lee, V. M., Goedert, M., and Trojanowski, J. Q. (2001) Neurodegenerative tauopathies. *Annu. Rev. Neurosci. 24*, 1121–1159.
(38) Brandt, R., Lee, G., Teplow, D. B., Shalloway, D., and Abdel-Ghany, M. (1994) Differential effect of phosphorylation and substrate modulation on tau's ability to promote microtubule growth and nucleation. *J. Biol. Chem. 269*, 11776–11782.
(39) Eidenmuller, J., Fath, T., Hellwig, A., Reed, J., Sontag, E., and Brandt, R. (2000) Structural and functional implications of tau hyperphosphorylation: information from phosphorylation-mimicking mutated tau proteins. *Biochemistry 39*, 13166–13175
(40) Leger, J., Kempf, M., Lee, G., and Brandt, R. (1997) Conversion of serine to aspartate imitates phosphorylation-induced changes in the structure and function of microtubule-associated protein tau. *J. Biol. Chem. 272*, 8441–8446
(41) Litersky, J. M., and Johnson, G. V. (1992) Phosphorylation by cAMP-dependent protein kinase inhibits the degradation of tau by calpain. *J. Biol. Chem. 267*, 1563–1568
(42) Hong, M., Zhukareva, V., Vogelsberg-Ragaglia, V., Wszolek, Z., Reed, L., Miller, B. I., Geschwind, D. H., Bird, T. D., McKeel, D., Goate, A., Morris, J. C., Wilhelmsen, K. C., Schellenberg, G. D., Trojanowski, J. Q., and Lee, V. M. (1998) Mutation-specific functional impairments in distinct tau isoforms of hereditary FTDP-17. *Science 282*, 1914–1917
(43) Vallee, R. B. (1982) A taxol-dependent procedure for the isolation of microtubules and microtubule-associated proteins (MAPs). *J. Cell Biol. 92*, 435–442
(44) Mandelkow, E. M., Drewes, G., Biernat, J., Gustke, N., Van Lint, J., Vandenheede, J. R., and Mandelkow, E. (1992) Glycogen synthase kinase-3 and the Alzheimer-like state of microtubule-associated protein tau. *FEBS Lett. 314*, 315–321
(45) Gamblin, T. C., King, M. E., Dawson, H., Vitek, M. P., Kuret, J., Berry, R. W., and Binder, L. I. (2000) In vitro polymerization of tau protein monitored by laser light scattering: Method and application to the study of FTDP-17 mutants. *Biochemistry 39*, 6136–6144
(46) Oosawa, F., and Asakura, S. (1975) Thermodynamics of the Polymerization of Protein , Academic Press, London.

(47) Janmey, P. A., Peetermans, J., Zaner, K. S., Stossel, T. P., and Tanaka, T. (1986) Structure and mobility of actin filaments as measured by quasielastic light scattering, viscometry, and electron microscopy. *J. Biol. Chem. 261*, 8357–8362.
(48) Augustinack, J. C., Schneider, A., Mandelkow, E. M., and Hyman, B. T. (2002) Specific tau phosphorylation sites correlate with severity of neuronal cytopathology in Alzheimer's disease. *Acta Neuropathol. 103*, 26–35.
(49) Schneider, A., Biernat, J., von Bergen, M., Mandelkow, E., and Mandelkow, E. M. (1999) Phosphorylation that detaches tau protein from microtubules (Ser262, Ser214) also protects it against aggregation into Alzheimer paired helical filaments. *Biochemistry 38*, 3549–3558.
(50) Connell, J. W., Gibb, G. M., Betts, J. C., Blackstock, W. P., Gallo, J., Lovestone, S., Hutton, M., and Anderton, B. H. (2001) Effects of FTDP-17 mutations on the in vitro phosphorylation of tau by glycogen synthase kinase 3β identified by mass spectrometry demonstrate certain mutations exert long-range conformational changes. *FEBS Lett. 493*, 40–44.
(51) Reynolds, C. H., Betts, J. C., Blackstock, W. P., Nebreda, A. R., and Anderton, B. H. (2000) Phosphorylation sites on tau identified by nanoelectrospray mass spectrometry: Differences in vitro between the mitogen-activated protein kinases ERK2, c-Jun N-terminal kinase and P38, and glycogen synthase kinase-3β. *J. Neurochem. 74*, 1587–1595.
(52) Ballatore, C., Lee, V. M., and Trojanowski, J. Q. (2007) Tau-mediated neurodegeneration in Alzheimer's disease and related disorders. *Nat. Rev. Neurosci. 8*, 663–672.
(53) Rankin, C. A., and Gamblin, T. C. (2008) Assessing the toxicity of tau aggregation. *J. Alzheimer's Dis. 14*, 411–416.
(54) Iqbal, K., Liu, F., Gong, C. X., Alonso, A. D., and Grundke-Iqbal, I. (2009) Mechanisms of tau-induced neurodegeneration. *Acta Neuropathol.* (in press).
(55) Alonso, A. C., Zaidi, T., Grundke-Iqbal, I., and Iqbal, K. (1994) Role of abnormally phosphorylated tau in the breakdown of microtubules in Alzheimer's disease. *Proc. Natl. Acad. Sci. U.S.A. 91*, 5562–5566.
(56) Alonso, A. C., Grundke-Iqbal, I., and Iqbal, K. (1996) Alzheimer's disease hyperphosphorylated tau sequesters normal tau into tangles of filaments and disassembles microtubules. *Nat. Med. 2*, 783–787.
(57) Li, B., Chohan, M. O., Grundke-Iqbal, I., and Iqbal, K. (2007) Disruption of microtubule network by Alzheimer abnormally hyperphosphorylated tau. *Acta Neuropathol. 113*, 501–511.
(58) Alonso Adel, C., Li, B., Grundke-Iqbal, I., and Iqbal, K. (2006) Polymerization of hyperphosphorylated tau into filaments eliminates its inhibitory activity. *Proc. Natl. Acad. Sci. U.S.A. 103*, 8864–8869.
(59) Santacruz, K., Lewis, J., Spires, T., Paulson, J., Kotilinek, L., Ingelsson, M., Guimaraes, A., DeTure, M., Ramsden, M., McGowan, E., Forster, C., Yue, M., Orne, J., Janus, C., Mariash, A., Kuskowski, M., Hyman, B., Hutton, M., and Ashe, K. H. (2005) Tau suppression in a neurodegenerative mouse model improves memory function. *Science 309*, 476–481.
(60) Berger, Z., Roder, H., Hanna, A., Carlson, A., Rangachari, V., Yue, M., Wszolek, Z., Ashe, K., Knight, J., Dickson, D., Andorfer, C., Rosenberry, T. L., Lewis, J., Hutton, M., and Janus, C. (2007) Accumulation of pathological tau species and memory loss in a conditional model of tauopathy. *J. Neurosci. 27*, 3650–3662.
(61) Spires, T. L., Orne, J. D., SantaCruz, K., Pitstick, R., Carlson, G. A., Ashe, K. H., and Hyman, B. T. (2006) Region-specific dissociation of neuronal loss and neurofibrillary pathology in a mouse model of tauopathy. *Am. J. Pathol. 168*, 1598–1607.